ACKNOWLEDGMENT

The authors wish to thank D. Tringali, C. Hooper, and C. Casau for their help with material growth and evaluation, and Dr. G. Antypas for the growth of InP substrate material. They also wish to thank R. Hendricks and T. Hierl for their assistance with device fabrication and evaluation.

REFERENCES

[1] K. W. Gray *et al.*, "Current limiting contacts for InP transferred electron devices," in *Proc. 5th Cornell Elect. Eng. Conf.*, pp. 215–244, 1975.
[2] D. J. Colliver, "Progress with InP transferred electron devices," in *Proc. 4th Cornell Elect. Eng. Conf.*, pp. 11–20, 1973.
[3] S. Baskaran and P. N. Robson, "Noise performance of InP reflection amplifiers in *Q*-band," *Electron. Lett.*, vol. 8, pp. 137–138, 1972.
[4] R. M. Corlett, I. Griffith, and J. J. Purcell, "Indium phosphide CW transferred electron amplifiers," *Electron Lett.*, vol. 10, pp. 307–308, 1974.
[5] J. E. Sitch, "Computer modelling of low noise indium phosphide amplifiers," *Electron. Lett.*, vol. 10, pp. 74–75, 1974.
[6] W. Fawcett and G. Hill, "Temperature dependence of the velocity/field characteristics of electrons in InP," *Electron. Lett.*, vol. 11, pp. 80–81, 1975.
[7] H. Kroemer, private communication.
[8] J. E. Sitch and P. N. Robson, "Noise measure of GaAs and InP transferred electron amplifiers," in *Proc. European Microwave Conf.*, 1974, London: Pitman Publishing, pp. 232–236.
[9] R. C. Clarke, B. D. Joyce, and W. H. E. Wilgors, "The preparation of high purity epitaxial InP," *Solid State Commun.*, vol. 8, pp. 1125–1128, 1970.
[10] B. Cairns and R. D. Fairman, "Effects of the $AsCl_3$ concentration on electrical properties and growth rates of vapor grown epitaxial GaAs," *J. Electrochem. Soc.*, vol. 115, p. 327C, 1968.
[11] ——, "Effect of the $AsCl_3$ concentration on impurity incorporation in vapor growth epitaxial GaAs," *J. Electrochem. Soc.*, vol. 117, p. 197C, 1970.
[12] R. C. Clarke, "A study of the molar fraction effect in the PCl_3–In–H_2 system," *J. Cryst. Growth*, vol. 23, pp. 166–168, 1974.
[13] M. J. Cardwell and R. F. Peart, "Measurement of carrier-concentration profiles in epitaxial indium phosphide," *Electron. Lett.*, vol. 9, pp. 88–89, 1973.
[14] L. J. Van der Pauw, "A method of measuring specific resistivity and hall effect of discs of arbitrary shape," *Philips Res. Rep.*, vol. 13, pp. 1–9, 1958.
[15] F. B. Fank and G. F. Day, "High CW power *K*-band Gunn oscillators," *Proc. IEEE* (Letter), vol. 57, pp. 339–340, 1969.
[16] J. G. de Koning *et al.*, "Gunn effect amplifiers for microwave communication systems in *X*, *Ku*, and *Ka*-bands," *IEEE Trans. Microwave Theory Tech.*, vol. MTT-23, pp. 367–374, 1975.
[17] T. G. Ruttan and R. E. Brown, "High frequency Gunn oscillators," in *Proc. Intl. Electron Devices Meeting*, Washington, DC, 1972.
[18] I. S. Groves and D. E. Lewis, "Resonant-cap structures for IMPATT diodes," *Electron Lett.*, vol. 8, pp. 98–99, 1972.
[19] T. G. Ruttan, "High frequency Gunn oscillators," *IEEE Trans. Microwave Theory Tech.*, vol. MTT-22, pp. 142–144, 1974.
[20] M. E. Hines, "Negative-resistance diode power amplification," *IEEE Trans. Electron Devices*, vol. ED-17, pp. 1–8, 1970.
[21] W. J. Getsinger, "Prototypes for use in broadbanding reflection amplifiers," *IEEE Trans. Microwave Theory Tech.*, vol. MTT-11, pp. 486–497, 1963.
[22] J. G. de Koning, R. E. Goldwasser, and S. I. Long, "Final technical report on full band transferred electron amplifiers," prepared for Naval Electronics Laboratory Center, San Diego, under contract N000123-74-C-0644, Feb. 1975.
[23] R. E. Goldwasser and F. E. Rosztoczy, "Gunn diodes for full band oscillators and amplifiers," *4th European Microwave Conf. Digest of Tech. Papers*, Montreux, Sept. 1974.
[24] The Plessey Co. Ltd, private communication.

Generation of Millimeter-Wave Signals of High Spectral Purity

ALFREDO A. CASTRO, MEMBER, IEEE, AND FRED P. ZIOLKOWSKI, MEMBER, IEEE

***Abstract*—The generation of millimeter-(mm-) wave signals phase coherent to a lower frequency reference or standard implies a large multiplication factor with inherent amplification of the short term instability or phase noise. This effect which usually is of secondary importance at lower microwave frequencies may become a limiting factor in the implementation of some mm-wave digital communication systems. Techniques used for the generation of signals of high spectral purity are discussed, and illustrated with the realization for a low data rate mm-wave satellite communications system. Quantitative results are presented and analyzed in terms of the theoretical time and frequency domain relationships.**

I. INTRODUCTION

THIS PAPER deals with the general theoretical considerations, approach, and state-of-the-art limitations for the generation of mm-wave signals of high spectral purity. It is well known that all frequency sources or generators exhibit frequency instabilities or fluctuations causing the instantaneous frequency $v(t)$ to be a random process with the addition of deterministic (hum, spurious, etc.) perturbations. As a result of these fluctuations, the ideal spectral line representing the frequency v_0 in the frequency domain will be broadened into a continuous power spectral density $S(f)$ plus the discrete lines representing the deterministic perturbations. Several terms and definitions are commonly used to characterize these frequency fluctuations such as long and short term stability, phase jitter, rms equivalent deviation, etc. Other definitions are used in the frequency domain to characterize spectral purity, such as phase and frequency noise power spectral density, sideband level with respect to the carrier, etc.

The sharpness of $S(f)$ is a graphical indication of the spectral purity of the frequency source. When this signal is angle modulated, the spectral broadening by frequency

Manuscript received February 2, 1976; revised May 10, 1976.
The authors are with the Communication Systems Laboratory, Raytheon Company, Sudbury, MA 01776.

instabilities inevitably results in information degradation. This effect will become more noticeable for the bottom baseband channels of FDM-FM radio relay systems and for low data rate digital modulation. The later case may be illustrated for a system at upper *Ka*-band that is PSK modulated at a symbol rate R. The standard deviation σ_ϕ of the phase instabilities over a signaling interval $1/R$ is

$$\sigma_\phi = 2\pi\nu_0\sigma_y(1/R)\cdot\frac{1}{R}. \tag{1}$$

This follows from the Allan variance $\sigma_y^2(\tau)$ definition in the following section. For the particular system described later in this paper, the measured data follow the curve fitting approximation $10^{-11}/\sqrt{\tau}$. For $\nu_0 = 40$ GHz, with equal transmit and receive instability contributions, substitution into (1) yields $\sigma_\phi \approx 3.5/\sqrt{R}$. Assuming a perfectly recovered carrier, the coherent demodulation of this signal with additive thermal noise is equivalent to the demodulation of an ideally modulated signal by a noisy reference having the same phase variance. Within certain approximations this later case, which has been treated elsewhere [1], shows that for $R = 150$ bit/s and BER $= 10^{-5}$, the Eb/No degradation is 2.2 dB. Furthermore, even in the absence of thermal noise, an irreducible BER floor will result.

If the carrier is recovered in a second-order loop of natural frequency f_n it may be shown using approximations developed in Appendix B that the σ_ϕ of the phase difference with respect to the received signal is

$$\sigma_\phi = \frac{\nu_0}{f_n}\sigma_y(1/\pi f_n) \tag{2}$$

which for the case being discussed becomes $\sigma_\phi = 0.7/\sqrt{f_n}$. By increasing the loop bandwidth, the recovered carrier will tend to follow the fluctuations of the received carrier. A penalty is paid, however, in that the phase variance due to the signal-to-thermal noise ratio in the loop will start to predominate. The best that can be hoped for is a compromise which minimizes the total phase variance due to both effects.

II. Spectral Purity Definitions

This section briefly summarizes the definitions for characterizing spectral purity which are used throughout. (See [2] for detailed treatment of this subject.) It is important at the onset to emphasize the duality that exists in the specification of spectral purity. The terminology of the title implies frequency domain; however, there is always a corresponding time domain representation.

2.1) Long and Short Term Stability Drift

A physical source of nominal frequency ν_0 has an instantaneous phase representable by $2\pi\nu_0 t + \phi(t)$ where $\phi(t)$ is a random process. Its first derivative is the instantaneous radian frequency fluctuation. All physical sources in differing degree exhibit drift, so that $\langle\dot{\phi}(t)\rangle \neq 0$. The presence of linear drift presents an immediate mathematical obstacle for the statistical definition of frequency stability (or spectral purity in the dual frequency domain). The perturbation is a nonergodic random process. This difficulty is removed by analyzing the time dependence of the second and third finite differences of the fractional fluctuation defined as

$$y(t) \equiv \frac{\dot{\phi}(t)}{2\pi\nu_0}. \tag{3}$$

It is measured by sampling the zero crossings over an interval τ every T seconds apart and averaging

$$\bar{y}_k = \frac{1}{\tau}\int_{t_k}^{t_k+\tau} y(t)\,dt = \frac{\phi(t_k+\tau)-\phi(t_k)}{2\pi\nu_0\tau}. \tag{4}$$

The fractional frequency variance between two adjacent sampling intervals of duration $\tau = T$ is of particular practical interest and is called the Allan variance

$$\langle\sigma_y^2(\tau)\rangle = \langle\tfrac{1}{2}(\bar{y}_1-\bar{y}_2)^2\rangle \approx \frac{1}{2M}\sum_{k=1}^{M}(\bar{y}_{k+1}-\bar{y}_k)^2. \tag{5}$$

This is the adopted definition of long and short term stability [2].

2.2) Definitions in the Frequency Domain

For small FM single tone disturbances to a frequency ν_0 at a deviation rate f, it is well known that the SSB power with respect to the carrier is $\hat{\phi}^2/4 = \phi_{\text{rms}}^2/2$. This notion can be extended to a random process to become the SSB spectral density with respect to the carrier level, and is denoted SSBC. Assuming a symmetrical distribution about ν_0, SSBC is one-half the one-sided power spectral density $S_\phi(f)$, which is the preferred definition [2]. Alternate forms of the same information about the noise process represented by the phase noise spectral density $S_\phi(f)$ are the frequency noise $S_{\Delta f}(f) = f^2S_\phi(f)$ and fractional frequency noise $S_y(f) = f^2S_\phi(f)/\nu_0^2$ spectral densities. Recently [3], the quantity $\mathcal{L}(f)$ has been introduced as a single-sideband measure of the total RF noise power. However, for system applications $S_\phi(f)$ or $S_{\Delta f}(f)$, whose integrals give the PM or FM noise power, is a more useful normalization. The square root of these integrated powers gives the phase and frequency jitter directly associated with that bandwidth.

2.3) Domain Transformation and Equivalence

It was mentioned at the beginning of this section that the time domain and frequency domain are merely different representations for the same phenomenon. If this is true then there ought to be a definite relationship between the two regimes. Unfortunately, due to the nonstationary statistics the well-known Wiener–Kintchine transformations for random processes cannot be applied here.

A formula due to Cutler and Searle enables such a transformation from the frequency domain to the time domain. It is basically a Fourier transform that involves the filtering effect, represented by a kernel function, due to the definition of the variance of the sampling process.

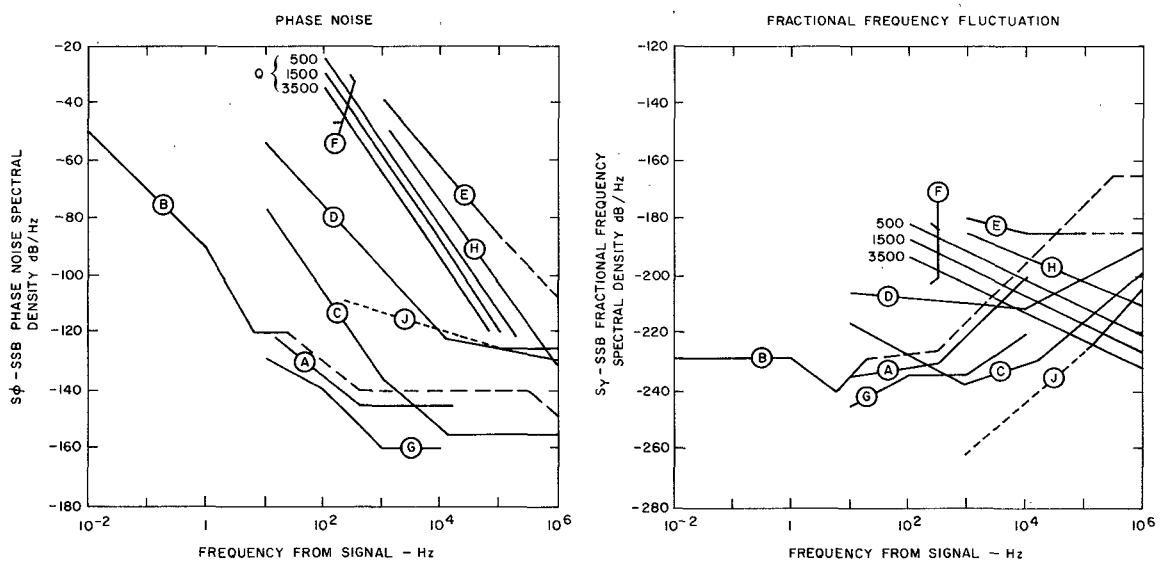

(a) (b)

Fig. 1. Short term frequency stability characteristics for frequency standards and VHF/microwave oscillators.

For the Allan variance this formula simplifies to

$$\langle \sigma_y^2(\tau) \rangle = \int_0^\infty Sy(f)K(u)\,df$$

$$K(u) = \frac{2\sin^4 u}{u^2} \qquad u = \pi f\tau. \tag{6}$$

Conversely, the spectral density may be derived from sampling in the time domain [4] by means of the Hadamard variance [5] σ_H^2

$$S_{\Delta f}(f) = \frac{N}{A_1^2 f}\sigma_H^2 - \left(\frac{A_3}{A_1}\right)^2 S_{\Delta f}(3f) - \left(\frac{A_5}{A_1}\right)^2 S_{\Delta f}(5f) - \cdots \tag{7a}$$

where

$$\sigma_H^2(N,T,\tau) = \langle (f_1 - f_2 + f_3 - \cdots - f_{aN})^2 \rangle \tag{7b}$$

$$A_j = 2N\frac{\sin j\pi\tau/2T}{j\pi\tau/2T},$$

$$j = 1,3,5, f = \frac{1}{2T}. \tag{7c}$$

This has practical application for close-in spectral measurements with computing counter instrumentation.

III. Physical Limitation of Devices Used for MM-Wave Generation

This section presents an overview of the spectral purity characteristics of physical devices used in the generation and amplification of mm-wave signals, where the long term stability is obtained by locking to primary or secondary standards. Reference oscillators and frequency standards, have a nominal frequency ν_0 in the HF to VHF range. Their principal attributes are a good combination of short and long term stability with emphasis on the latter. For a given system, all the signals generated are ultimately related to it in a coherent manner by frequency multiplication. One of the unavoidable and undesirable consequences of this multiplication process is that the noise fluctuations are multiplied as well as the signal. This multiplicative phase noise degradation represents the minimum degradation that can be incurred. Physical devices can also incur increased noise of a nonmultiplicative nature that is referred to as additive or excess phase noise. Measurement of a high level multiplier from *X* to upper *Ka* band indicates excess noise that is typically 40 dB below the multiplicative noise. A properly designed times *N* multiplier up to mm-wave frequencies increases the phase or frequency noise of the driving source by an N^2 factor, with negligible addition of excess noise.

Fig. 1(a) illustrates the phase noise characteristics of the devices listed in Table I which can be used to drive multiplier chains or to generate mm-wave frequencies. Direct com-

TABLE I
Oscillator Characteristics

DESCRIPTION/TYPE	CURVE
5 MHz COMPONENT OSCILLATOR	A
5 MHz RUBIDIUM ATOMIC STANDARD	B
5 MHz DISCIPLINED TIME FREQUENCY STANDARD	G
100 MHz CRYSTAL OSCILLATOR	C
400 MHz VCO .01% TUNABILITY	D
X-BAND GUNN Q_L = 500, 1500, 3500	F
X-BAND GUNN - 550 MW 0.8% TUNABILITY (VCO)	H
X-BAND IMPATT - 10 MW	E
X-BAND INJECTION LOCKED IMPATT 550 MW - 0.8% TUNABILITY (VCO)	J

parison is expedited by using the fractional frequency power spectral density $S_y(f)$, which is invariant under frequency multiplication. This is done in Fig. 1(b) from which a number of general conclusions may be derived:

a) different devices offer better spectral noise characteristics in different regions;
b) the magnitude of the tunability of oscillators introduces unavoidable degradation of the spectral characteristics;
c) the spectral characteristics of solid-state bulk oscillators improve with the value of the loaded Q of the microwave cavity.

When an oscillator having a phase noise spectral density $S_\phi(f)$ is phase locked to an ideal reference, its $S_\phi(f)$ at the output is multiplied by $|1 - H(f)|^2$. Here $H(f)$ is the closed loop transfer function, which behaves as a low-pass filter. When phase locked to a real signal, the close-in spectral characteristics at the output of the VCO will follow the phase fluctuations of the driving signal, but will have its own characteristics for frequencies beyond the loop bandwidth. Similar behavior results in an injection locked oscillator where the transition frequency is controlled by the cavity Q and the output to injection power ratios [7]. Therefore, by phase and injection locking oscillators at different frequencies, followed by multiplication, the spectral characteristics at mm-wave frequencies may be improved with respect to the one attainable by only multiplication of a low frequency primary or secondary standard. This technique is illustrated in the realization discussed in the next section.

Other factors external to the oscillation process itself result in random and deterministic phase noise in addition to the inherent oscillator noise. These are caused by shock and vibration, power supply ripple, electric and magnetic strays pickup, spurious signal generated by the frequency synthesis process, coupling of amplitude to phase modulation in active devices, etc.

Mechanical stresses resulting from vibration induce dimensional changes which couple into electronic perturbations. The sensitivity of an oscillator to vibration is usually defined by an experimentally determined vibration pushing factor α_v. A fractional frequency change $\Delta f/\nu_0$ is induced per unit of acceleration which is taken to be g_e (earth gravitational field)

$$\alpha_v \equiv \frac{\Delta f}{\nu_0}\frac{1}{g/g_e}. \tag{8}$$

The vibration induced frequency excursions in the one-sided spectral density are given by

$$S_y^{\nu_k} = \tfrac{1}{2}(\alpha_v g/g_e)^2. \tag{9}$$

Here $S_y^{\nu_k}$ are either delta function weights at the mechanical eigenfrequencies $\nu_{1,2,3}$, or may have an arbitrary continuous frequency distribution.

All physical devices exhibit a sensitivity to the biasing or dc voltages which will induce phase fluctuations due to the ripple and perturbations in the power supplies. In oscillators,

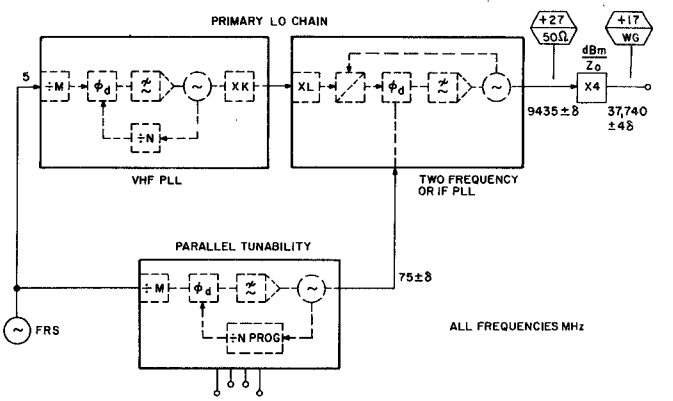

Fig. 2. Block diagram of tunable LO chain with parallel tunability for high spectral purity.

this sensitivity is usually given by a pushing factor $\alpha_r = \Delta f/\Delta V$ in hertz/volt. For amplifiers, the sensitivity of the device to the power supply voltages is given by a pushing factor related to the dynamic change of the output signal phase with respect to the input dc voltages $\alpha_r = \Delta\phi/\Delta V$ giving

$$S_\phi^{\,v} = (\alpha_r \Delta V_{\text{rms}})^2. \tag{10}$$

Stray magnetic fields, radiated emissions, line pickup represent any of a number of other possible sources of spurious pickup. Their significance as a problem depends on the particular equipment used and the manner of its configuration. If any such factor is identified as a problem, one would seek to measure or determine from previous effort, appropriate sensitivity or pushing factors. Since all active devices (and ferrite devices in some instances) have an AM/PM coefficient, amplitude modulation in the signals used in the generation of spectrally pure signals should be avoided.

Finally, active devices in oscillators or amplifiers may generate spurious signals which when close to the desired frequency degrade the spectral purity or stability. Spurious signals which fall into this category are ion beam oscillations in thermoionic devices and parametric oscillation spurs in varactor multipliers and IMPATT diodes.

IV. Satellite Communications Applications

Fig. 2 gives the block diagram of the low noise millimeter-wave frequency generation equipment that was implemented. It utilizes a master 5-MHz crystal reference oscillator which is "cleaned up" by serially placed phase-locked loops closed around very quiet VHF and SHF oscillators. The 5-MHz crystal can in turn be phase locked to an atomic standard to significantly reduce the long term drift by several orders of magnitude. The crux of the approach in Fig. 2 is the use of the dual reference phase-locked loop (IFPL) which enabled the design to functionally separate the high stability design from the tunability requirements in the parallel chain. At the point of combination within the IFPL, the primary chain has accrued approximately a 40 dB of phase noise increase over the parallel tunable chain by virtue of the increased multiplication. This allows con-

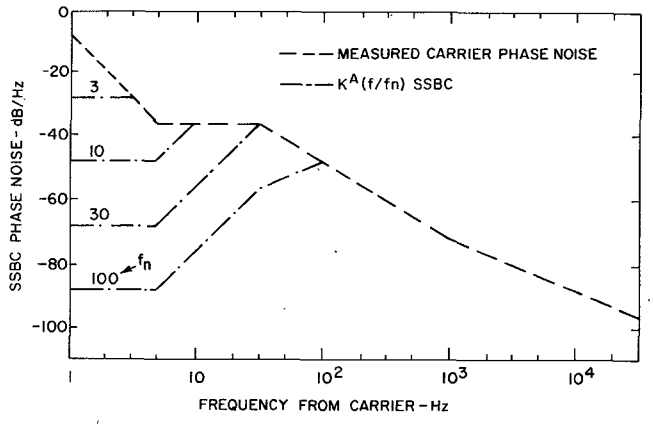

Fig. 3. Measured SSBC data at K-band and $K^4(f/fn) \times$ SSBC for selected values of $f_n = (\pi\tau)^{-1}$.

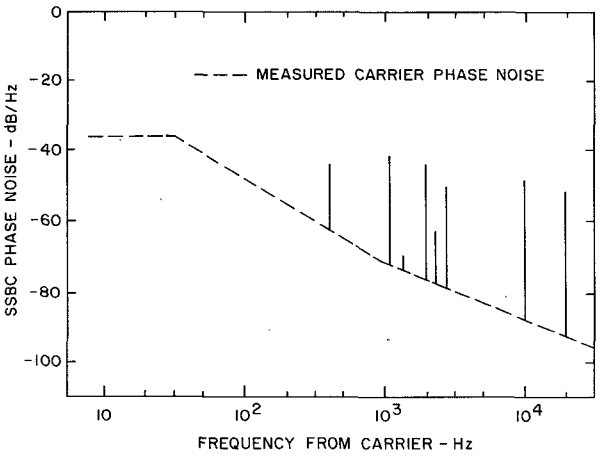

Fig. 5. Measured SSBC at transmitter output at Ka-band.

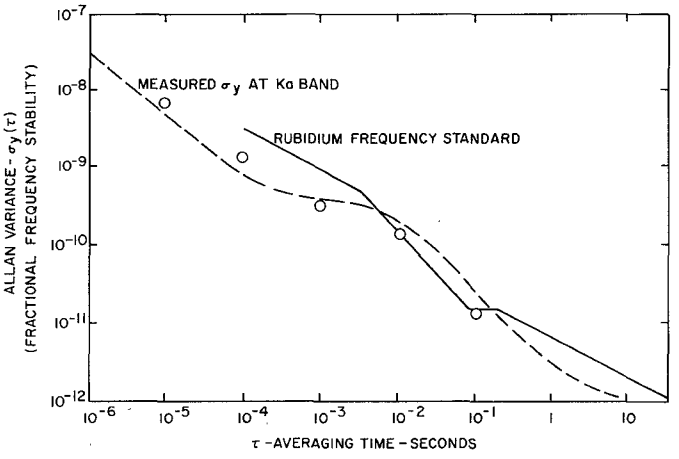

Fig. 4. Measured Allan variance $\sigma_y(\tau)$ and computed values 0 from S_ϕ data of Fig. 3.

siderable margin for the degradation of the secondary chain due to the tunability. Attempting mixing and filtering at the RF frequency rather than utilizing the two frequency loop would be much more difficult particularly in view of the half-watt required to drive the final X4 multiplication to K band.

Although only a moderate amount of tunability ($\sim$1 percent) was implemented, the approach given in Fig. 1 is essentially the same that may be utilized in the construction of wider bandwidth microwave synthesizers. The key component is a YIG tuned Gunn oscillator which is presently available at frequencies up to 40 GHz.

4.1) Performance Data and Analysis

Figs. 3 and 4 give the independently measured S_ϕ and σ_y data for the frequency generation equipment of Fig. 2. It is an interesting and meaningful exercise to verify their consistency by use of the Cutler–Searle domain transformation introduced in Section II. The details of the method are outlined in Appendix A. The computed values are given in Fig. 4 by the dots. The agreement is considered to be quite good, particularly in view of the instrumentation difficulties.

Fig. 5 shows the spectral measurements at the output of the transmitter system [8], in which the discrete spurious due to the power supply ripple lines and its harmonics are apparent. Their effect relative to that of the random noise of the frequency generation process is obtained by integrating their separate contributions. Computation indicates the discrete of Fig. 5 contributes 0.02-rad rms to the continuous spectrum (10 Hz to 25 kHz) phase jitter of 0.15-rad rms.

V. Summary and Conclusions

Spectral purity at mm-wave frequencies becomes an important consideration for some applications due to the inherent degradation in the phase noise or short term stability caused by the large multiplication factor required in generating these signals. The existence of a performance threshold due to the source's short term frequency instability indicates careful attention of the spectral purity associated with the carrier, particularly at lower data rates, angle modulated communication systems.

The mm-wave devices exhibit fractional frequency noise characteristics similar to the ones at lower microwave frequencies; however, the absolute magnitude of the degradations are roughly proportional to the square of the frequency ratio. By the use of injection or phase-locked oscillators at certain critical frequencies, a substantial improvement of the overall spectral purity of mm-wave signal with respect to straight multiplication of a lower frequency reference may be obtained. Also, by proper synthesis, frequency agility may be incorporated, without appreciable spectral purity degradation.

The quantitative specification and measurement of the spectral purity, and the evaluation of the degradation caused to a particular information modulation scheme, require the use of a number of parametric definitions in both time and frequency domain, and to establish its equivalence and domain transformation. The nonstationary statistics of the frequency fluctuation process complicate these definitions and the domain transformation.

A low noise design that was implemented at K-band frequencies is given along with the independently measured

analog $S_\phi(f)$ and digital $\sigma_y(\tau)$-carrier noise representations. By use of approximate formulas developed for nonclassical distributions in the Cutler–Searle equation, agreement is demonstrated. It is believed that the design described and its experimental results, are representative of the state of the art of high spectral purity mm-wave generation required in a low data rate satellite communications. However, the general principles can be extended to other applications such as Doppler radar and tracking.

Appendix A
Approximate Evaluation of Cutler–Searle Equation for Nonclassical Distributions

Under the assumption that $S_\phi(f)$ is known locally in the vicinity of $f_n = (\pi\tau)^{-1}$ and representable by $S_\phi(1)f^{-\gamma}$ for arbitrary γ between 1.5 and 5, a simple "slide rule" approximate evaluation of the Cutler–Searle equation for $\sigma_y^2(\tau)$ is given. Here $S_\phi(1)$ denotes $S_\phi(f = 1)$. Results developed for arbitrary $\gamma < 1.5$ require specification of an additional parameter f_c. Results for integer γ that correspond to the classical white, flicker, and random walk distributions have been published [2]. However, the application to nonclassical distributions that result from actual synthesis procedures, particularly when those distributions are irregular as in Fig. 3, were not previously available.

It follows from (6) upon substituting $S_y = f^2 S_\phi \nu_0^{-2}$ and $S_\phi(f) = S_\phi(1)f^{-\gamma}$ that

$$\sigma_y^2(\tau) = \frac{2S_\phi(1)}{(\pi\tau\nu_0)^2}\frac{C^\infty(\gamma)}{f_n^{\gamma-1}} \tag{A1}$$

where

$$C^\infty(\gamma) = \int_0^\infty \frac{K'(u)}{u^\gamma}\,du \tag{A2}$$

and $K'(u) = \sin^4 u$. For $\gamma = 2$, 3, and 4, $C^\infty(\gamma)$ can be evaluated exactly with values of $\pi/4$, $2 \ln 2$, and $\pi/3$, respectively.

The dotted line of Fig. 6 plots $K'(u)$ and an approximation to it $K^A(u)$ identified by the dashed line and defined by u^4 for $u \le 1$ and unity for $u > 1$. The difference between $K^A(u)$ and $K'(u)$ is accounted for by introducing a correction factor c. An important characteristic of the integral is the corner frequency f_n that is directly related to the averaging time τ by $f_n = (\pi\tau)^{-1}$.

Utilizing a piecewise approximation to $S_\phi(f)$ above and below f_n gives

$$K^A \cdot S_\phi(f) = S_\phi(1)\begin{cases} f^{-\gamma}, & f_n \le f \\ f^\lambda f_n^{-\lambda-\gamma}, & f < f_n. \end{cases} \tag{A3}$$

Assuming a high frequency cutoff f_c for $S_\phi(f)$, the integral (A2) $K'(u) \approx K^A(u)$, becomes

$$C(\lambda,\gamma,f_c) = c\left(\frac{1}{1+\lambda} + \frac{f_n^{\gamma-1}}{1-\gamma}(f_c^{1-\gamma} - f_n^{1-\gamma})\right), \qquad \gamma \neq 1 \quad \lambda > -1. \tag{A4}$$

Here c is a correction factor that for $0 \le \gamma \le 5$ is bounded by 3/8 and unity if $f_c \gg f_n$. If $\gamma > 2$, or $\gamma > 1$ and $f_c \gg f_n$ this simplifies to

$$C(\lambda,\gamma) = c\left(\frac{1}{1+\lambda} + \frac{1}{\gamma-1}\right), \qquad \gamma \neq 1 \quad \lambda > -1. \tag{A5}$$

If $\lambda = 4 - \gamma$ as would occur if $S_\phi(1)f^{-\gamma}$ is locally valid about f_n, the results simplify further to

$$C(\gamma) = c\frac{4}{(5-\gamma)(\gamma-1)}, \qquad 1 < \gamma < 5. \tag{A6}$$

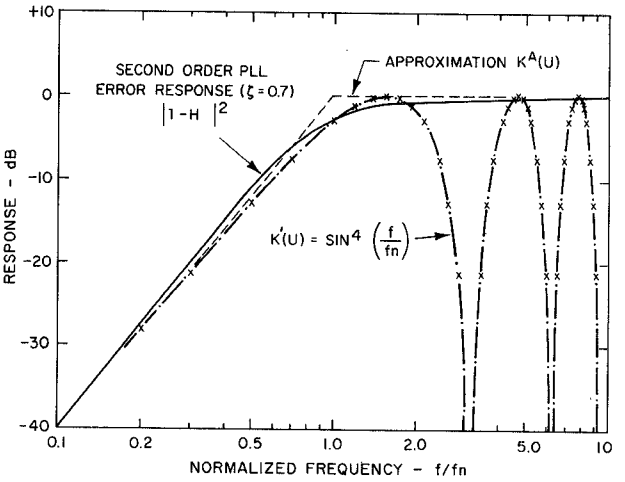

Fig. 6. Comparison of the exact kernel function $K'(u) = \sin^4 u$ for Cutler–Searle equation and approximation $K^A(u)$.

TABLE II

γ	$C^\infty(\gamma)$ $f<f_n$	$f_n<f$	$\sigma_y^2(\tau)$	c
0 TO 1*	—	—	$\frac{0.202\ S_\phi(1)}{\nu_0^2\ \tau^2}\ \frac{c}{1-\gamma}\ f_c^{1-\gamma}$ *	0.375 TO 0.46
1	—	—	$\frac{0.202\ S_\phi(1)}{\nu_0^2\ \tau^2}\ \ell n\, f_c/f_n$ *	0.46
1.5	0.286	2.00	$\frac{0.82\ S_\phi(1)}{\nu_0^2\ \tau^{3/2}}$	0.51
2.0	1/3	1	$\frac{0.85\ S_\phi(1)}{\nu_0^2\ \tau}$	0.56
2.5	0.40	0.667	$\frac{1.2\ S_\phi(1)}{\nu_0^2\sqrt{\tau}}$	0.62
3.0	1/2	1/2	$\frac{2\ S_\phi(1)}{\nu_0^2}$	0.68
3.5	0.667	0.40	$\frac{3.78\ S_\phi(1)\sqrt{\tau}}{\nu_0^2}$	0.76
4.0	1	1/3	$\frac{8.4\ S_\phi(1)\tau}{\nu_0^2}$	0.84
4.5	2.00	0.286	$\frac{26\ S_\phi(1)\tau^{3/2}}{\nu_0^2}$	0.92

* ASSUMES $f_c \gg f_n$

TABLE III
MEASURED K-BAND S_ϕ DATA—37 GHz (PER FIG. 3)

f - Hz	γ	$S_\phi(1)$ dB
1 to 5	4	-5
5 to 30	0	-33
30 to 10^3	2.4	+3
10^3 to 3 x 10^4	1.65	-19

An approximate algorithm for c deduced from the exact results for integer γ assuming $f_c \gg f_n$ is $0.375e^{0.2\gamma}$. Table II gives expressions for half-integer values of γ in the range (1.5, 4.5). Additional results for (0, 1) require the parameter f_c explicitly in addition to $S_\phi(1)$ and γ. The approximate correction factor c is identified in the last column.

By using Table III for the S_ϕ data of Fig. 3, the computed values of in Fig. 4 were obtained assuming $c = 1$.

APPENDIX B
USE OF $\sigma_y(\tau)$ TO MODEL ERROR RESPONSE OF SECOND-ORDER PHASE-LOCKED LOOP

Inspection of the curves in Fig. 6 indicate that the Cutler–Searle kernel $K'(u) = \sin^4 u$ approximates the error response of a second-order phase-locked loop.

Substitution of $|1 - H(f)|^2$ for $\sin^4 u$ into (6) while noting that $S_y(f) = f^2 S_\phi(f)/\nu_0^2$ and $f_n = (\pi\tau)^{-1}$ yields (2) directly, after accounting for equal contributions from the T_x and R_x phase noise.

ACKNOWLEDGMENT

The realization discussed in Section IV was done under the Air Force Avionics Laboratory Contract F33615-73-C-4036, T. Joyner, Project Engineer. Most of the experimental data were obtained with the collaboration of E. Perdue and L. Serulneck, both from Raytheon, and R. Hazel, presently at MITRE.

REFERENCES

[1] J. J. Stiffler, *Theory of Synchronous Communications*. Englewood Cliffs: Prentice Hall, 1971, ch. 9.
[2] NBS Technical Note 394, "Characterization of frequency stability," Oct. 1970.
[3] NBS Technical Note 632, "Frequency stability specification and measurement: High frequency and microwave signals," Jan. 1973.
[4] R. Blackman and J. Tukey, *The Measurement of Power Spectra*. New York: Dover, 1959.
[5] R. Bough, "Frequency modulation analysis with the Hadamard variance," presented at the Frequency Control Symp., Apr. 1971.
[6] F. Gardner, *Phaselock Techniques*. New York: Wiley, 1966.
[7] M. Hines, J. Collinet, and J. Ondria, "FM noise suppression of an injection phase locked oscillator," *IEEE Trans. Microwave Theory Tech.*, vol. MTT-16, Sept. 1968.
[8] A. Castro and J. Healy, "Transmitter system for mm-wave satellite communication," presented at the IEEE Int. Commun. Conf., 1975.

A Versatile Millimeter-Wave Imaging System

JAMES P. HOLLINGER, JAMES E. KENNEY, AND BALLARD E. TROY, JR.

***Abstract*—A new millimeter-wave imaging system has been assembled at the Naval Research Laboratory and flight-tested using the NASA/Wallops C-54 aircraft. The system incorporates an oscillating mirror and interchangeable radiometer units making it particularly adaptable to variations in its operational frequency, polarization, and angular resolution. Flight tests of the system have been conducted at 90 GHz and simultaneously at 22 and 31 GHz using a dual frequency radiometer. The imaging system and data processing are described and some of the initial flight test results at 90 GHz are presented.**

INTRODUCTION

PASSIVE microwave imagers have proved to be of great value for the remote sensing of the environment. Various imagers at 10, 19, and 37 GHz have been instrumented and flown aboard aircraft for a wide range of environmental investigations. Two electrically scanning microwave radiometers (ESMR) are currently in use aboard satellites; the 19-GHz ESMR on Nimbus 5 and the 37-GHz ESMR on Nimbus 6. Also on Nimbus 6 is the scanning microwave spectrometer (SCAMS), operating at 22.2, 31.4, 52.85, 53.85, and 55.45 GHz, which employs mechanically scanned reflectors. Microwave imagers have been used in meteorology to infer the thickness and water content of clouds and to map the location and distribution of fronts, convective zones, storms, and areas of precipitation. They have been used to delineate the ice–ocean edge; to locate icebergs, polynyas, and leads; to identify and map ice type and coverage; and to detect and quantify marine oil spills. Over land they have provided information on soil moisture and located field and vegetation boundaries, roads, railroads, and commercial, industrial, residential, and open areas. In addition maps of agricultural, geological, and geographical features have been obtained even at night and even through a snow cover.

Manuscript received December 5, 1976; revised May 4, 1976.
The authors are with the Space Science Division, Naval Research Laboratory, Washington, DC 20375.